Experimental investigation on interaction between extreme waves and a submerged barrier

Liang Kong(),[1] Xiaochen Li(),[1] Hongchao Lu(),[2] Kang Ren(),[3] Ying Gao(),[4] and Kun Liu()[1, a)]

[1)] *School of Civil Engineering and Transportation. South China University of Technology, Guangzhou 510630, PR China*

[2)] *College of Marine Science and Technology, China University of Geosciences, Wuhan, 430074, PR China*

[3)] *Department of Mechanical Engineering, University College London, Torrington Place, London WC1E 7JE, United Kingdom*

[4)] *Imperial College London, Department of Earth Science & Engineering, Exhibition Rd, South Kensington, London SW7 2BX, United Kingdom*

(Dated: 3 February 2024)

We present experimental results of a group of focused waves propagating over a submerged barrier positioned in various locations on the bottom of a flume. The study investigates the effect of the relative distance between the fixed focusing position and different barrier installation positions on the characteristics of the wave group. The surface elevation and skewness are observed to approach a crest just on top of the barrier's rear. It can be also suggested that the presence of the barrier may affect the evolution of the wave group for approximately two times of the barrier length, as indicated by the frequency component distribution. In the time domain, a small tail with mildly higher energy is generally observed when the gauge is fixed at the front surface of the barrier. It suggests that long waves at lower frequencies propagate at higher speeds, while short waves at higher frequencies are intercepted due to the barrier.

[a)] Electronic mail: liukun86@scut.edu.cn

I. INTRODUCTION

Rogue waves, also known as freak waves, are characterized by abnormally large wave heights, occurring unpredictably at various times and locations[1,2]. The mechanisms driving the generation of rogue waves are complicated[3], with factors such as alterations in the topography, wave-current interaction, and wind-wave interaction, which can potentially lead to wave energy focusing, resulting in the occurrence of rogue waves due to reflection or refraction phenomena[4,5]. In addition, when waves propagate from deep to shallow water, bottom non-uniformity can also provoke significantly increased probability of rogue waves generation[6].

In the field of marine engineering, the investigation of rogue waves is crucial due to the considerable energy they carry, posing threats to ocean structures[7]. This concern is particularly relevant in the context of the growing development of floating offshore wind turbines globally, necessitating comprehensive studies on the interaction between rogue waves and structures. Various methods have been commonly employed in the study of rogue waves, including physical experiments, numerical simulations, ,and theoretical investigations[8–10]. For instance, McAllister *et al.*[11] recreated the Draupner wave's characteristics in a circular wave tank, observing that large crossing angles between wave systems were crucial for accurately reproducing its scaled crest and total wave height. Fernandez and Sriram[12] used a Self Correcting Method (SCM) to generate accurate focused wave by optimizing the wave maker's motion, validated by physical experiments. High order spectral (HOS) methods have been introduced to calculate the probability of abnormal waves occurrence under different conditions[13–16]. Moreover, artificial intelligence had been applied to the study of rogue waves.

The interaction between ocean structures or topography and waves or currents has garnered significant attention. The literature on wave-structure interaction expands beyond rogue waves. Analytical investigation has delved into diverse scenarios based on linearized assumptions, encompassing the study of the interaction between free surface waves and elastic structures[17], and the coupling of hydroelastic waves with rigid structures[18,19]. These investigations collectively contribute to a comprehensive understanding of the intricate dynamics between waves and structures in various environmental scenarios. In addition, numerical simulation is widely adopted in the study of non-linear wave-structure interaction,

as demonstrated by the work of Peng *et al.*[20] and Shi and Zhu[21]. In the realm of solitory waves, earlier studies, exemplified by Mei and Black[22], simplified structures and topography. Based on that, advanced techniques, such as those employed by Chang, Hsu, and Liu[23], conducted experiments and numerical simulations to study the interaction between solitary waves and submerged rectangular obstacles. Ghafari *et al.*[24] introduced two obstacles into a wave tank under solitary waves, revealing the presence of a clockwise vortex between the obstacles and the occurrence of wave breaking when the waves propagated between them, as observed through Particle Image Velocimetry (PIV). Li *et al.*[25] investigated the wave propagation atop ADTs in intermediate water depth by modeling the system based on the second-order theory. They claimed that the second-order free waves caused by the ADTs played an important role in the generation of the rogue wave. Geng, Liu, and Dias[26] placed a horizontal plate underwater to find that the shape of the solitary wave propagating by the plate was modified and focused at the end of the plate. Brossard *et al.*[27] conducted experimental studies in a wave tank to examine the decomposition of monochromatic waves on a submerged plate, revealing that the submerged plate is a more effective barrier for first and second-order wave characteristics. Chang[28] studied the generation and evolution of vortices around submerged rectangular obstacles under elliptical waves experimentally and numerically. It showed that the wave period influenced the vortex strength significantly. In addition to considering the extreme waves in the environmental input, the resonant waves[29–31] whose spectrum constantly evolves during the propagation process may also produce a large load on the structure.

In contrast to previous research, our study investigates the effect of the relative distance between the wave focusing position and barrier on the focused wave characteristics. The paper is organized as follows: In Sec. II, the experimental setup is described. In Sec. III we investigate the characteristics of the focused waves, including the surface elevation, skewness and kurtosis, frequency distribution, and the energy distribution in the time domain. Finally, the conclusions are summarized in Sec. IV.

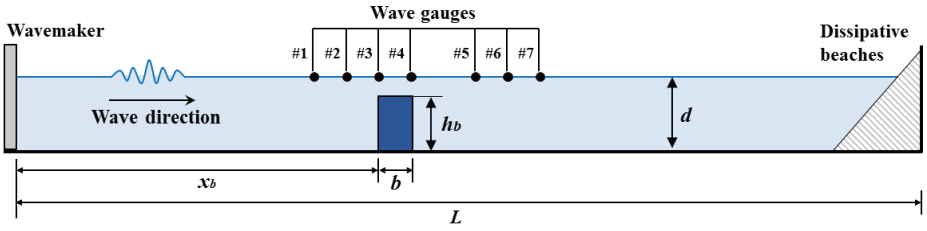

FIG. 1. Schematic of the experimental setup including wavemaker, wave gauges, barrier, and dissipative beaches.

II. DESCRIPTION OF THE EXPERIMENTS

A. Experimental Setup

The experiments were carried out in the laboratory at the China University of Geosciences, and the experimental setup is shown in Fig. 1. A wave flume, with $L = 50$m in length, $B = 1$m in width, and $D = 1.5$m in height, was filled with water to a depth of $d = 1.0$m. On one side of the wave flume, a piston-type wavemaker was installed, while the opposite side featured of a relaxation zone containing wave-absorbing sponges. A wooden cuboid barrier, with dimensions $h_b = 0.8$m in height, $b = 0.5$m in length and $l_b = 1$m in width (as same as the width of the wave flume), was firmly placed on the bottom of the wave flume. Partially filled with lead weight for stability during experiments, the barrier could be moved along the longitudinal direction of the flume to accommodate various scenarios.

Wave trains with frequencies ranging from 0.75Hz to 1.25Hz were generated as incident waves. To concentrate them into a focused wave group at a specific location, a constant amplitude distribution was employed. We selected wave groups focused at the fixed position $L_f = 16.0$m and time $T_f = 30$s, each with one of five different focused amplitudes A_f as input. Throughout the experiments, we kept the wave group's focused position constant, systematically adjusting the barrier's position x_b in 0.5m increments within the range from 15.5m to 19m.

The water surface elevation was simultaneously measured using seven capacitive wave gauges, each operating at a sampling frequency of 20Hz. These gauges were strategically positioned at various positions x_g along the flume, corresponding to distances from the

TABLE I. Experimental parameters (d=1.0m)

Case No.	A_f(m)	x_b(m)
A1-A8	0.03	
B1-B8	0.04	
C1-C8	0.05	15.5, 16.0, 16.5, 17.0, 17.5, 18.0, 18.5, 19.0
D1-D8	0.06	
E1-E8	0.07	

wavemaker's resting position as follows: 15.5m(#1), 16.0m(#2), 16.5m(#3), 17.5m(#4), 18.0m(#5), 18.5m(#6), 19.0m(#7). To ensure accuracy, three experiments were conducted for each scenarios, and the data were averaged. The key parameters for the main set of the experiments are detailed in table I , each assigned a specific case ID to identify different conditions.

III. EXPERIMENTAL RESULTS

A. Surface Elevation

To examine the impact of the prescribed wave amplitude on surface elevation, a series of experiments were performed with five wave amplitudes, namely, 0.03m, 0.04m, 0.05m, 0.06m, and 0.07m. With the barrier fixed at a consistent position on the bottom, it was observed that the maximum elevation η_{max} for each specified amplitude A_f reached a crest at the focused position L_f and subsequently decreased. However, it then approached another crest at the rear of the barrier before decreasing again. Taking $x_b = 16.5$m as an example in Fig. 2, it is evident that the maximum elevation η_{max} measured by this gauge is smaller than that by the gauges in front of and behind it.

Given the consistent trend in free surface elevation at different designed focused amplitudes, the focus shifted to examining the effect of barrier position. In the following investigation, identical incident wave trains with $A_f = 0.05$m as the designed amplitude propagated over the barrier installed at various positions ranging from 15.5m to19m, as listed in cases C1-C8 in Table I. The dimensionless maximum surface elevation η_{max}/A_f is depicted in Fig. 3. For all cases except case C2 with $x_b = 16$m, it reaches a maximum

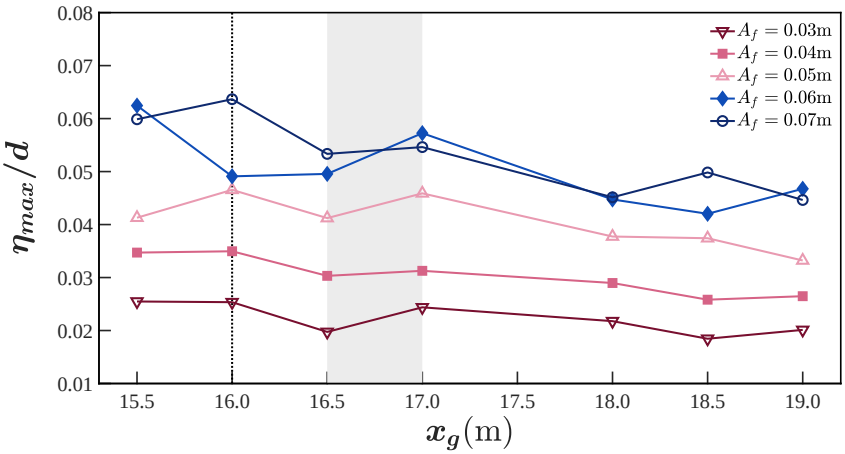

FIG. 2. Dimensionless surface elevation η_{max}/d measured by 7 gauges versus designed amplitude A_f with a barrier located at $x_b = 16.5$m. Grey region denotes the barrier position, while black dashed lines show the designed focused position.

value at $x_f = 16$m, the designated focused place, before decreasing significantly with the longitudinal coordinate.

Notably, the dimensionless maximum elevation measured by the gauge just at the rear of the barrier is greater than the data measured by both the gauges after it and at the front of the barrier, resulting in a crest in the data. This discrepancy is the principal cause of the shift in the maximum value in case C2.

Fig. 3 also reveals that the dimensionless maximum wave height H_{max}/A_f follows a similar trend. The data measured by the gauge at the rear of the barrier also reaches a crest. However, the difference between H_{max}/A_f and η_{max}/H_{max} at the front and the rear of the barrier are approximately the same. This illustrates that the variation of the trough can be ignored, and the non-linearity of the wave group becomes stronger during this process. To further illustrate this phenomenon, the asymmetric coefficients η_{max}/H_{max} versus cases are shown in Fig. 3. For all cases, this coefficient reaches or is closed to a crest at the rear of the barrier, consistent with the earlier conclusion. It is worth noting that for case C2 with $x_b = x_f = 16$m, the asymmetric coefficient is even mildly enhanced, indicating that the non-linearity of the wave group continues to grow for at least twice the length of the barrier

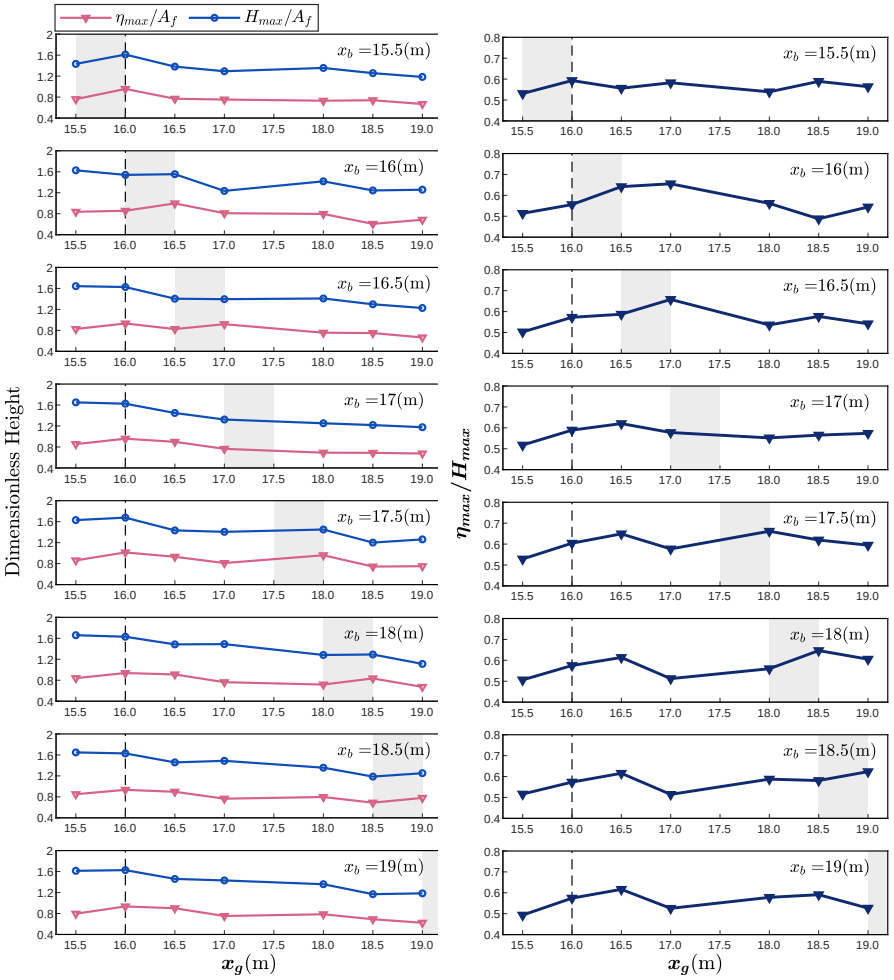

FIG. 3. The left column shows evolution of dimensionless maximum surface elevation and dimensionless wave height versus different barrier position with $A_f = 0.05$m; The right column the ratio of them. Grey region denotes the barrier position, while black dashed lines show the designed focused position.

after propagating over it.

B. Skewness and Kurtosis

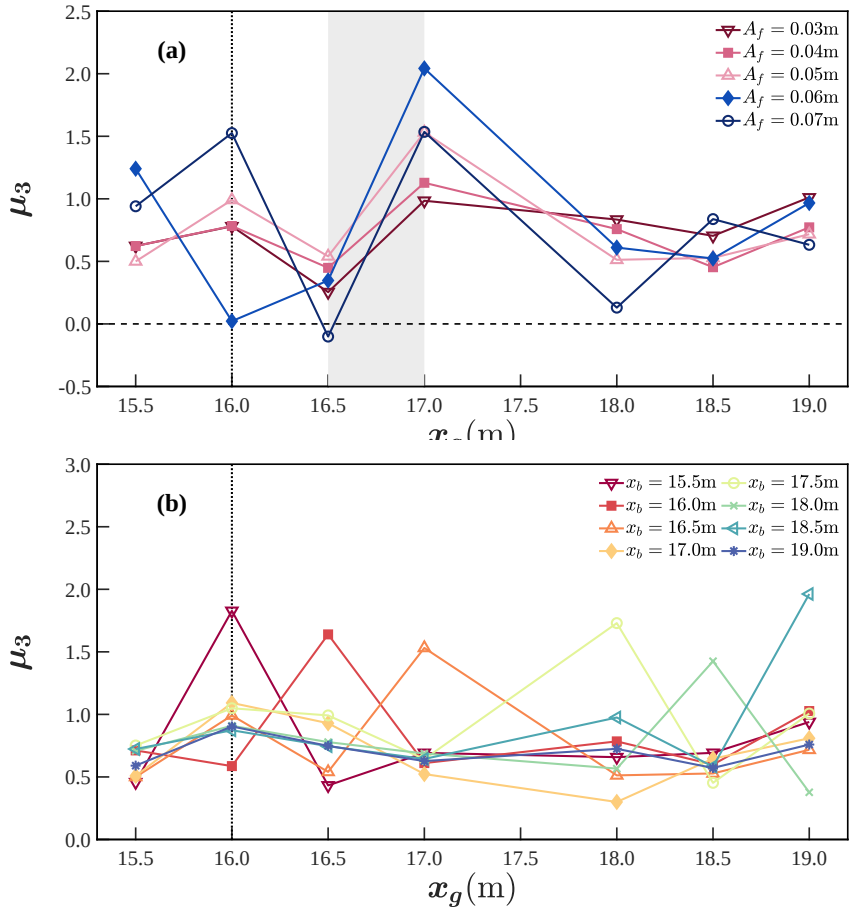

FIG. 4. Evolution of skewness (a) with a fixed barrier position$x_b = 16.5$m. (b) with a fixed designed focus amplitude $A_f = 0.05$m.The barrier is represented by the grey area, and the designated focused position is marked by a black vertical dotted line.

To study the statistical characteristics of the group of focused waves, skewness and kurtosis are calculated to assess their distribution and behavior. Skewness represents wave profile asymmetry around the vertical axis, while kurtosis denotes the probability of rogue wave occurrence.

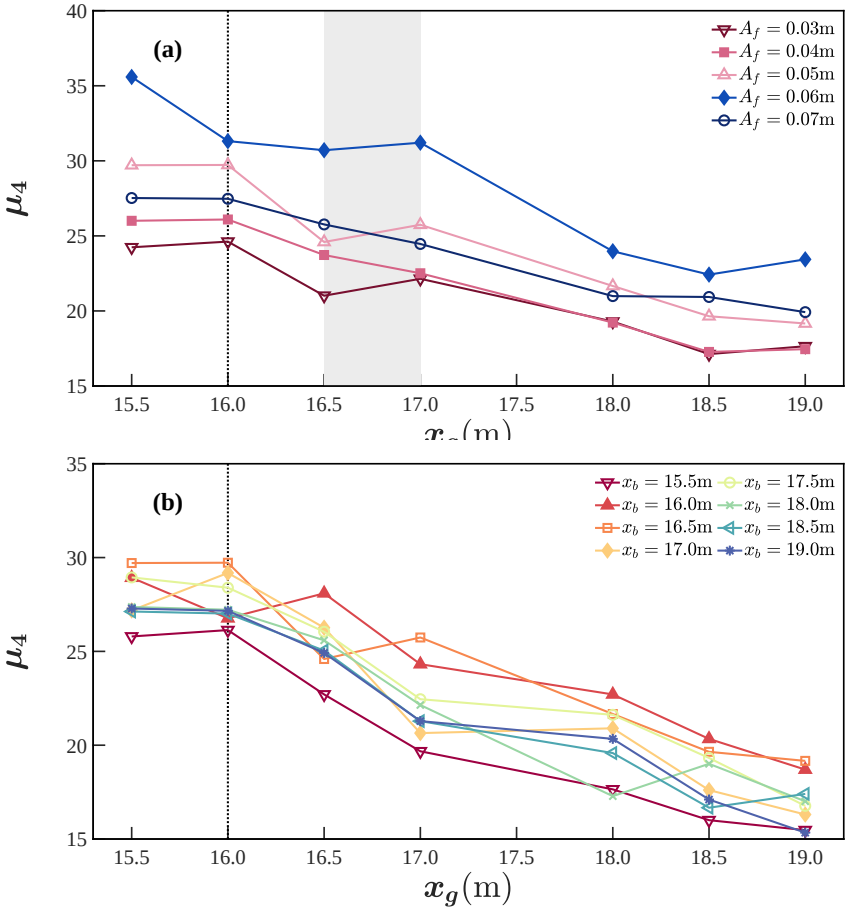

FIG. 5. Evolution of kurtosis: (a) with a fixed barrier position $x_b = 16.5$m. (b) with a fixed designated focus amplitude $A_f = 0.05$m. The barrier is represented by the grey area, and the designated focused position is marked by a black vertical dotted line.

The skewness of the free surface elevation is given by:

$$\mu_3 = \frac{\langle(\eta - \langle\eta\rangle)^3\rangle}{\sigma^3} \tag{1}$$

and the Kurtosis of the free surface elevation is defined as:

$$\mu_4 = \frac{\langle(\eta - \langle\eta\rangle)^4\rangle}{\sigma^4} \tag{2}$$

where$\langle\cdot\rangle$ is the averaging operator, and $\sigma^2 = \langle(\eta - \langle\eta\rangle)^2\rangle$ for η being the surface elevation.

The evolution of skewness is shown in Fig. 4. For different A_f in the range from 0.03m to 0.07m with the barrier placed at x_b=16.5m, the skewness reaches its minimum just at x_g = 16.5m, then peaked at the next gauge. This suggests that the wave packet consistently tended to the right, given that the skewness remained greater than 0. To investigate the effect of the barrier position on skewness, cases C1-C8 with a fixed A_f=0.05m are shown in Fig 4(a). It is evident that the skewness peaks at the gauge on top of the rear of the barrier.

Fig.5 shows the evolution of kurtosis. When the barrier is installed at x_b=16.5m, the value descends along the flume for different A_f in the range from 0.03m to 0.07m as shown in Fig5(b). It first decreases at x_g = 16.5m, and then recovers at the next gauge, to form a mild crest in the curve. If we fix A_f=0.05m and move the barrier in the range from 15.5m to 18.5m at a step of 0.5m, the trough exists at the gauge behind the barrier. The observation that the skewness and the kurtosis increases when the wave packet passed the barrier aligns with the conclusion drawn from the surface elevation, suggesting modulation during this progress.

C. The Frequency Components

To delve deeper into the harmonic and super-harmonic components of the surface elevation with the barrier installed at different positions, the data is segregated using the Fast Fourier Transform (FFT) method into different orders. Taking case C3 with x_b = 16.5m as an example, the energy spectra are presented in Fig. 6(a). It can be observed from the curves for all seven gauges that the energy concentrated in the main range of 0.75Hz-1.25Hz averagely. However, the energy in the main range decreases while the energy of second-order increases mildly along the direction of propagation. Notably, the energy near three times this range is approximately three orders of magnitude smaller than the main range, suggesting that three-order effects may be neglected in such circumstance.

From the super-harmonic part, there is a plateau near 1.5Hz and then a gap near 1.7Hz for the gauges 1-3 in front of the barrier. However, just behind the barrier, at gauge 4, the super-harmonic energy differs significantly from gauge 1-3, aligning with the variation

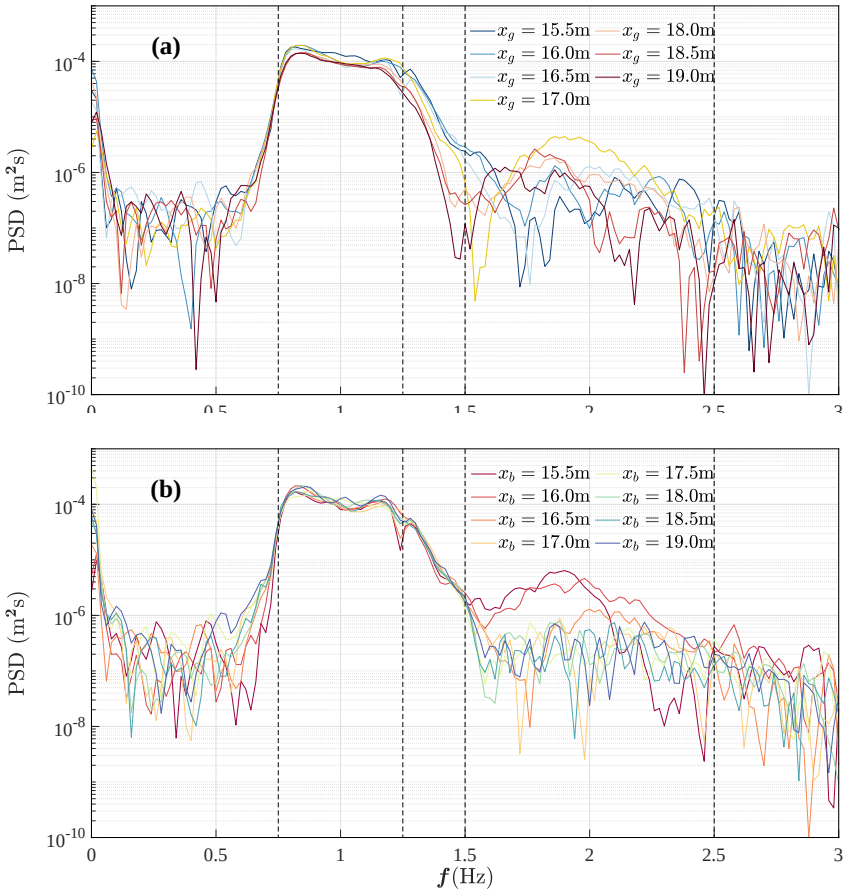

FIG. 6. Energy spectra of surface elevation versus frequency: (a) at different gauge positions for case C3 with $x_b = 16.5$m (b) at gauge 3 for case C1-C8. Here, $A_f = 0.05$m.

of the maximum elevation. A gap occurs in the energy spectra curve near 1.5Hz instead of the plateau, while a larger crest rises at approximately 2Hz. After the barrier, the crest decreases, and the energy tends to distribute evenly mildly.

To illustrate the effect of the barrier bottom, the energy spectra for cases C1-C8 measured by gauge 3 are provided in Fig 6(b). For all these eight cases, the wave groups are designed to focus to a fixed amplitude at the same position, while the barrier is installed at different places. It can be observed that for case C1 and C2, the wave group has already passed the

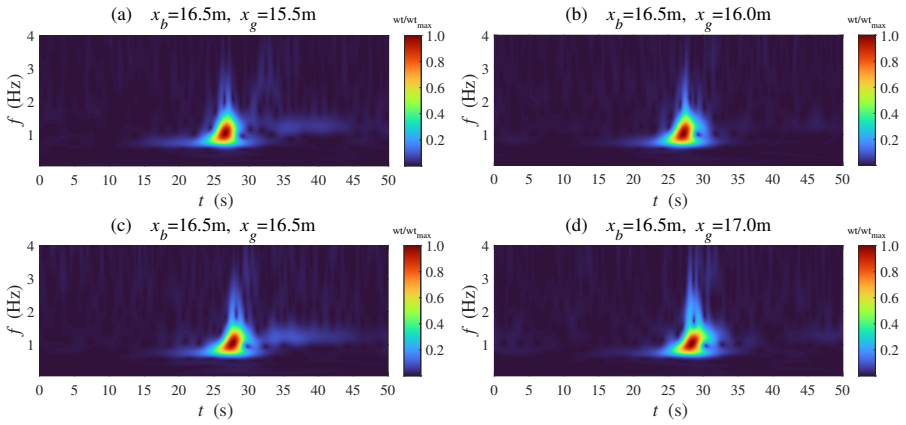

FIG. 7. Wavelet transform analysis of time series of free surface elevation when x_b=16.5m and A_f=0.05m.

barrier, and the energy in the second-order range is significantly larger than other cases. If we move the barrier to the position under gauge 3, as in case C3, the second-order energy decreases remarkably, and an energy gap occurs at approximately 1.8Hz. For case C4-C8, considering the wave group focused at a certain distance away from the barrier, there is no obvious difference between them. This result also suggests that the effect of the barrier may persist for approximately two times the barrier length.

D. Wavelet Analysis

To perform a more in-depth investigation into the mechanism of energy transfer among different frequencies, we employ wavelet transform (WT) technique to study the energy distribution of waves in the time domain.

For the case with barrier positioned 16.5m away from the wave maker and the focused amplitude A_f designed to be 0.05m, there is an area of energy focusing in the frequency from 0.5Hz to 2Hz during the time interval 20s-30s, as shown in Fig. 7. For the data measured by the four gauges around the focused place, the concentration of wave energy occurs primarily in the range from 0.75Hz to 1.25Hz, which is the designated frequency region. It then extends to 0.5Hz-4Hz; however, most of the energy still remains in the range of the first-

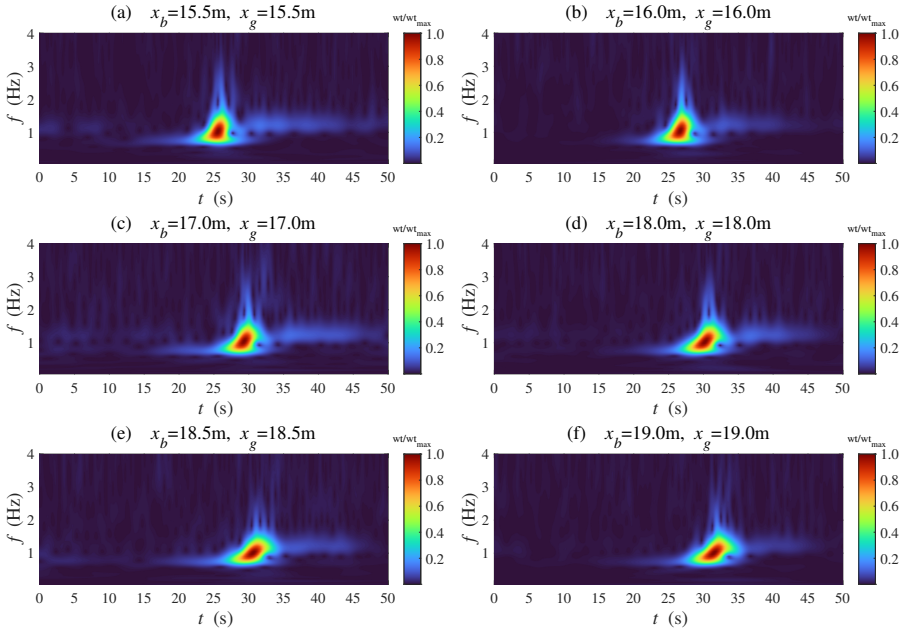

FIG. 8. Wavelet transform analysis of time series of free surface elevation when the barrier and the gauge are at the same position $x_b = x_g$ with A_f=0.05m.

order frequency. It is obvious that the energy concentration region inclines to the right gradually in propagation, especially after the barrier, which suggests that the long waves at lower frequency propagate at a higher speed than the short waves at higher frequency due to the barrier. Therefore, a long tail at the frequency in the range from 1Hz to 2Hz appears at Gauge 3 and lasts from 32s to 37s, which has not been observed at the adjacent gauges 2 and 4. It suggests that the waves at higher frequency are intercepted although the barrier is emerged in water.

Additional cases shown in Fig. 8 demonstrate that the small area of higher energy generally exists when the gauge and the front of the barrier are fixed at the same place. In addition, the length of these areas appears to decrease mildly with the displacement away from the focused place, likely due to energy dissipation along the flume.

IV. CONCLUSION

An experimental investigation was conducted to assess the impact of the relative distance between the fixed focusing position and various positions of the installed barrier on the characteristics of the wave group. Throughout the experimental campaign, we performed 40 cases under 8 carrier positions. Our key findings indicate that, among the seven gauges, the surface elevation reaches a crest at the rear of the barrier. This observation suggests that the effect of the barrier may endure for approximately twice its length, which is supported by the distribution of frequency components. In addition, the observation that the skewness and the kurtosis increase as the wave packet passes the barrier suggests modulation during this progress. In the time domain, the results demonstrate that long waves at lower frequencies exhibit higher propagation speeds, while short waves at higher frequencies are intercepted due to the presence of the barrier.

ACKNOWLEDGMENTS

This work was supported by the Key-Area Research and Development Program of Guangdong Province (No. 2020B1111010001), Guangdong Basic and Applied Basic Research Foundation (Nos. 2022A1515012417 and 2023A1515030138), the Fundamental Research Funds for the Central Universities (No. 2022ZYGXZR034) and the Marine Economic Development of Guangdong, China (No.GDNRC[2021]39).

DECLARATION OF INTERESTS

The authors report no conflict of interest.

DATA AVAILABILITY

The data that supports the findings of this study are available within the article and from the corresponding author upon reasonable request.

REFERENCES

[1]C. Viotti and F. Dias, "Extreme waves induced by strong depth transitions: Fully nonlinear results," Phys. Fluids **26**, 287–310 (2014).

[2]I. Georgescu, "The great rogue wave," Nat. Phys. **9**, 526–526 (2013).

[3]D. R. Solli, C. Ropers, P. Koonath, and B. Jalali, "Optical rogue waves," Nature **450**, 1054–1057 (2007).

[4]T. A. Adcock and P. H. Taylor, "The physics of anomalous ('rogue') ocean waves," Rep. Prog. Phys. **77**, 105901 (2014).

[5]M. Onorato, S. Residori, U. Bortolozzo, A. Montina, and F. Arecchi, "Rogue waves and their generating mechanisms in different physical contexts," Phys. Rep. **528**, 47–89 (2013).

[6]G. O, Z. H, and T. K, "Freak waves in weakly nonlinear unidirectional wave trains over a sloping bottom in shallow water," Phys. Fluids **25**, 097101–319 (2013).

[7]K. Dysthe, H. E. Krogstad, and P. Müller, "Oceanic rogue waves," Annu. Rev. Fluid Mech. **40**, 287–310 (2008).

[8]T. Tang, D. Barratt, H. B. Bingham, T. S. van den Bremer, and T. A. Adcock, "The impact of removing the high-frequency spectral tail on rogue wave statistics," J. Fluid Mech. **953**, A9 (2022).

[9]G. Ducrozet, F. Bonnefoy, and P. Ferrant, "On the equivalence of unidirectional rogue waves detected in periodic simulations and reproduced in numerical wave tanks," Ocean Eng. **117**, 346–358 (2016).

[10]C. Lawrence, K. Trulsen, and O. Gramstad, "Statistical properties of wave kinematics in long-crested irregular waves propagating over non-uniform bathymetry," Phys. Fluids **33**, 046601 (2021).

[11]M. L. McAllister, S. Draycott, T. Adcock, P. Taylor, and T. Van Den Bremer, "Laboratory recreation of the draupner wave and the role of breaking in crossing seas," J. Fluid Mech. **860**, 767–786 (2019).

[12]H. Fernandez and V. Sriram, "Extreme wave generation using self correcting method — revisited," Coastal Eng. **93**, 15–31 (2014).

[13]L. Wang, K. Ding, B. Zhou, J. Li, S. Liu, and T. Tang, "Quantitative prediction of the freak wave occurrence probability in co-propagating mixed waves," Ocean Eng. **271**, 113810 (2023).

[14]L. Wang, J. Li, S. Liu, and G. Ducrozet, "Statistics of long-crested extreme waves in single and mixed sea states," Ocean Dyn. **71**, 21–42 (2021).

[15]L. Wang, K. Ding, B. Zhou, P. Jin, S. Liu, J. Wang, and T. Tang, "Nonlinear statistical characteristics of the multi-directional waves with equivalent energy," Phys. Fluids **35** (2023).

[16]L. Wang, J. Li, S. Liu, and Y. Fan, "Experimental and numerical studies on the focused waves generated by double wave groups," Front. Energy Res. **8**, 133 (2020).

[17]K. Ren, G. X. Wu, and Y. F. Yang, "Surface wave interaction with floating elastic plates in channels," Phys. Fluids. **36**, 017143 (2024).

[18]K. Ren, G. X. Wu, and C. Y. Ji, "Diffraction of hydroelastic waves by multiple vertical circular cylinders," J. Eng. Math. **113**, 45–64 (2018).

[19]Q. Y. Wu, T. I. Khabakhpasheva, B. Y. Ni, and A. A. Korobkin, "Small-amplitude waves in a floating poroelastic plate forcing by vertical pitching plate," Phys. Fluids. **35**, 117127 (2023).

[20]N. N. Peng, W. K. Lau, O. W. H. Wai, and K. W. Chow, "Computational and experimental studies of wave–structure interaction: Wave attenuation by a floating breakwater," Phys. Fluids. **35**, 045112 (2023).

[21]K. Shi and R. Zhu, "Efficient spectral coupled boundary element method for fully nonlinear wave–structure interaction simulation," Phys. Fluids. **35**, 057121 (2023).

[22]C. C. Mei and J. L. Black, "Scattering of surface waves by rectangular obstacles in waters of finite depth," J. Fluid Mech. **38**, 499–511 (1969).

[23]K. Chang, T. Hsu, and P. L. F. Liu, "Vortex generation and evolution in water waves propagating over a submerged rectangular obstacle: Part i. solitary waves," Coastal Eng. **44**, 13–36 (2001).

[24]A. Ghafari, M. R. Tavakoli, M. Nili-Ahmadabadi, K. Teimouri, and K. C. Kim, "Investigation of interaction between solitary wave and two submerged rectangular obstacles," Ocean Eng. **237**, 109659 (2021).

[25]Y. Li, S. Draycott, Y. Zheng, Z. Lin, T. A. Adcock, and T. S. van den Bremer, "Why rogue waves occur atop abrupt depth transitions," J. Fluid Mech. **919**, R5 (2021).

[26]T. Geng, H. Liu, and F. Dias, "Solitary-wave loads on a three-dimensional submerged horizontal plate: Numerical computations and comparison with experiments," Phys. Fluids **33**, 037129 (2021).

[27]J. Brossard, G. Perret, L. Blonce, and A. Diedhiou, "Higher harmonics induced by a submerged horizontal plate and a submerged rectangular step in a wave flume," Coastal Eng. **56**, 11–22 (2009).

[28]K. A. Chang, "Vortex generation and evolution in water waves propagating over a submerged rectangular obstacle: Part i. solitary waves," Coastal Eng. **44**, 13–36 (2001).

[29]J. Y. Li, Z. Liu, S. J. Liao, and G. L. B. Alistair, "Steady-state multiple near resonances of periodic interfacial waves with rigid boundary," Phys. Fluids. **32**, 087104 (2020).

[30]J. Y. Li, Z. Liu, S. J. Liao, and G. L. B. Alistair, "Steady-state harmonic resonance of periodic interfacial waves with free-surface boundary conditions based on the homotopy analysis method," J. Fluid Mech. **916**, A58 (2021).

[31]J. Y. Li, H. L. Su, Z. Liu, and X. C. He, "Steady-state interfacial gravity waves with one-dimensional class-iv triad resonance." Phys. Fluids. **35**, 092104 (2023).